NASA Technical Paper 2919

1989

Interactions of Tollmien-Schlichting Waves and Dean Vortices

Comparison of Direct Numerical Simulation and a Weakly Nonlinear Theory

Bart A. Singer
High Technology Corporation
Hampton, Virginia

Thomas A. Zang
Langley Research Center
Hampton, Virginia

National Aeronautics and Space Administration
Office of Management
Scientific and Technical Information Division

1. Introduction

The study of incompressible curved channel flow can illuminate some important issues dealing with laminar-turbulent transition. The streamwise curvature of the flow induces an instability resulting in longitudinal vortices (hereafter referred to as Dean vortices (ref. 1)). For mildly curved channels, the minimum Reynolds number for instability of the Dean vortices is comparable with that for Tollmien-Schlichting (TS) waves. In this regime, Gibson and Cook (ref. 2) showed that oblique waves are never the dominant linear disturbance. This makes the flow an ideal candidate for studying the nonlinear interactions between two-dimensional (2D) TS waves and the streamwise-oriented Dean vortices. The fact that the flow is strictly parallel implies that a self-consistent analysis can be performed without the application of triple-deck theory (ref. 3).

To date, the only weakly nonlinear theory for the interaction of Dean vortices and TS waves at finite Reynolds numbers is that developed by Daudpota, Hall, and Zang (hereafter referred to as DHZ) (ref. 3). They employ a multiple-scale version of the Stuart (ref. 4) and Watson (ref. 5) approach to approximate the complex equations describing the flow as two coupled Landau equations for the perturbation amplitudes of Dean vortices and TS waves. These Landau equations are examined in the context of a nonlinear autonomous system (for details on nonlinear autonomous systems see, for example, ref. 6) to determine the characteristics of the various equilibrium states (nodes). Using this information, one can make predictions about the behavior of the real flow for ranges of parameters. The limits of these ranges are not known a priori; they must be determined by some other means. Direct numerical simulation (DNS) of the full equations describing the flow can be used to check the validity of the theory at specific points in the parameter space. In this paper we use DNS to determine the accuracy of the weakly nonlinear theory developed by DHZ.

In section 2 we enumerate the relevant nomenclature and describe the weakly nonlinear theory. Section 3 describes the DNS code with which we compare the weakly nonlinear predictions. We compare the results in section 4 and discuss their implications in section 5.

The authors would like to thank Q. Isa Daudpota and Philip Hall for their many useful discussions associated with this project.

2. Mathematical Formulation of the Weakly Nonlinear Theory

Here we introduce the notation and scalings used in the weakly nonlinear theory. The notation is the same as that used by DHZ. The interested reader is referred there for a detailed description of the theory; here we give only the information that is essential for its application.

Cylindrical coordinates (r, θ, z) are used to describe the flow between infinite concentric walls of outer radius R_o and inner radius R_i. Figure 1 illustrates the geometry of the problem. The distance between the walls $d = R_o - R_i$ is used to nondimensionalize the axial (spanwise) coordinate z, while the outer radius R_o nondimensionalizes the radial coordinate r. The ratio $\eta = R_i/R_o$ is used to describe the curvature of the channel; the radial coordinate r varies between η and 1. The quantity $1 - \eta$ appears often and is denoted by λ. At the critical curvature parameter $\lambda_c = 2.179 \times 10^{-5}$, the minimum Reynolds number for instability of TS waves is the same as that for Dean vortices (see Gibson and Cook, ref. 2). When plotting velocity distributions in the radial direction, it is convenient for the abscissa to vary between -1 and 1, hence we define another radial coordinate, $y = (2r - (1 + \eta))/\lambda$.

The mean flow is denoted by radial velocity U, azimuthal velocity V, axial velocity W, and pressure P. When a constant azimuthal pressure gradient $\frac{\partial P}{\partial \theta}$ drives the flow, a solution to the momentum equations gives (U, V, W) as

$$\begin{pmatrix} U \\ V \\ W \end{pmatrix} = \begin{pmatrix} 0 \\ V_m f(r) \\ 0 \end{pmatrix} \tag{1}$$

where[1]

$$V_m = -\frac{R_o}{2\nu\rho}\frac{\partial P}{\partial \theta}\lambda^2 \tag{2}$$

$$f(r) = -\frac{\eta}{\lambda^2}\left[r\log r + \frac{\eta^2 \log \eta}{r(1-\eta^2)}(r^2-1)\right] \tag{3}$$

The kinematic viscosity ν and the density ρ are constant. The Reynolds number is defined as

$$Re = \frac{V_m d}{\nu} \tag{4}$$

In the limit of a straight channel, V_m becomes four times the mean centerline velocity, and the Reynolds number approaches eight times the standard straight channel Reynolds number based on centerline velocity and half-width.

The mean flow described above is disturbed with pressure p and velocity (u, v, w) perturbations. The perturbation pressure is scaled with ρV_m^2, the radial and axial velocities with the diffusive scale ν/d, and the azimuthal velocity v with the convective velocity scale V_m. Time t is normalized with R_o/V_m.

On the neutral stability curve the linear perturbations due to the Dean vortex are proportional to $\epsilon \exp(ikz)$, where ϵ is an arbitrary small parameter, $i = \sqrt{-1}$, and the spanwise wave number k is scaled with channel width d. Linear TS disturbances are proportional to $\epsilon \exp(im\theta)\exp(\sigma t)$, where the nondimensional complex growth rate σ is defined as

$$\sigma = \sigma_R + i\sigma_I \tag{5}$$

and $\sigma_R = 0$ on the TS neutral stability curve. The dimensional streamwise wave number for a TS wave, α_{TS}, is related to the wave number m via the relation

$$\alpha_{\mathrm{TS}} dx = m d\theta \tag{6}$$

where dx is the differential distance along the centerline of the channel. Hence, using

$$dx = \frac{R_i + R_o}{2} d\theta \tag{7}$$

one obtains the relation

$$d \cdot \alpha_{\mathrm{TS}} = 2\frac{1-\eta}{1+\eta} m \tag{8}$$

where the quantity d is included so that α_{TS} has the appropriate dimensions. Note that $d \cdot \alpha_{\mathrm{TS}}$ is nondimensional such that its value is twice the standard straight channel value of the nondimensional streamwise wave number.

Neutral stability curves for TS and Dean disturbances for curvatures slightly less than, equal to, and slightly greater than the critical value are shown in figures 2(a) and (b). The apparent sensitivity of the TS disturbances to curvature is an artifact of using m as the abscissa. Using the transformation equation (8) one finds that the plots overlap; differences in the value of the neutral Reynolds number for a given TS wavelength are less than 20 for the three cases shown. For the Dean disturbances, differences in the neutral Reynolds number are about 200. For consistency with standard nomenclature, the left branch of these curves will be called the lower branch and the right side will be called the upper branch. Reference 3 concentrates on the lower branch of the TS neutral

[1] Typographical errors in DHZ account for a missing factor of η in their definition of $f(r)$.

curve because it is the more relevant branch when one considers boundary-layer-type flows. In the case of the Dean instability, harmonics of the lower branch wave number can fall in the unstable region and actually grow faster than the primary disturbance considered by the weakly nonlinear theory. To avoid this possibility, here we restrict our attention to the Dean upper branch.

The Reynolds number is expanded about a value R_0 that is on both the TS and the Dean neutral stability curves so that

$$Re = R_0 + \epsilon^2 R_1$$

The curvature parameter Λ is written as a deviation from the critical curvature ratio at which the minimum Reynolds number is the same for TS and Dean disturbances. Hence

$$\lambda = \lambda_c + \epsilon^2 \Lambda$$

A slow time variable is defined by

$$\tau = \epsilon^2 t$$

The quantity $\epsilon X(\tau)$ represents the time history of half the maximum azimuthal velocity of the Dean vortex, evaluated on the channel centerline. The corresponding quantity for TS waves is $\epsilon Y(\tau)$, which measures half the maximum radial velocity on the centerline. The following coupled set of Landau equations were derived by DHZ:

$$\frac{1}{2}\frac{d|X|^2}{d\tau} = (R_1\beta_1 + \Lambda\gamma_1)|X|^2 + \delta_1|X|^2|X|^2 + \eta_1|X|^2|Y|^2 \tag{9}$$

$$\frac{1}{2}\frac{d|Y|^2}{d\tau} = (R_1\beta_2 + \Lambda\gamma_2)|Y|^2 + \delta_2|Y|^2|X|^2 + \eta_2|Y|^2|Y|^2 \tag{10}$$

The ratios $-\gamma_1/\beta_1$ and $-\gamma_2/\beta_2$ are the slopes of the zero-growth-rate curves for $|X|$ and $|Y|$ in the (Λ, R_1) plane. Numerical computations (confirmed by us) indicate that $\Lambda\gamma_2 << R_1\beta_2$ for all cases considered, so γ_2 is taken to be zero in what follows. The seven remaining coefficients, γ_1, β_1, β_2, δ_1, δ_2, η_1, and η_2, are all computed at points where the Dean and TS neutral stability curves intersect. These values were computed by DHZ, using 51 points across the channel with a fourth-order finite-difference discretization. We used the same software and recomputed the coefficients, using 501 points across the channel. All but the coefficient η_2 remained constant to three digits with the increased resolution; η_2 changed by about 20%.

Equations (9) and (10) admit four possible steady state solutions: the trivial solution, finite $|X|$ with $|Y| = 0$, finite $|Y|$ with $|X| = 0$, and a combined state with finite values of both $|X|$ and $|Y|$. Each of these states is a critical point and may be classified according to the local behavior of the solutions in the vicinity of the point. In the phase plane ($|X|$ - $|Y|$), stable nodes are identified as those for which solution trajectories near the point converge to the node, unstable nodes are critical points from which solution trajectories diverge, and saddle points are those points for which a finite number of trajectories converge to the point while all others diverge. For the case of a channel more strongly curved than critical ($\Lambda > 0$), DHZ found that the trivial solution is an unstable node, the TS equilibrium state is a saddle point, and the Dean equilibrium state is a stable node. No combined mode solution exists here. For any initial condition that contains even a very small amplitude Dean disturbance, the solution will ultimately tend towards an equilibrium Dean disturbance with no TS perturbation. The situation with $\Lambda < 0$ is more complicated. For small Reynolds number deviations from the neutral curve, only the TS equilibrium state will exist. At larger deviations, the TS state itself is unstable and the combined state of TS and Dean disturbances is stable. For sufficiently large Reynolds number perturbations, only the equilibrium Dean disturbance will persist.

3. The Direct Numerical Simulation

Here we describe the numerical techniques used to solve the full Navier-Stokes equations in the curved channel. The basic equations are written in perturbation variables; the total velocity is

$(U,V,W)+(u^*,v^*,w^*)$, where (U,V,W) are given by equations (1)–(3) of section 2. The coordinates and velocities are then nondimensionalized with the outer radius of curvature R_o and the quantity V_m, which is defined in equation (2). Primed variables are the nondimensional counterparts of the respective starred quantities. In primitive variable form, the continuity and momentum equations are

$$0 = \frac{1}{r}\frac{\partial(ru')}{\partial r} + \frac{1}{r}\frac{\partial v'}{\partial \theta} + \frac{\partial w'}{\partial z} \tag{11}$$

$$\frac{\partial u'}{\partial t} = (f+v')\left(\frac{1}{r}\frac{\partial(ru')}{\partial r} - \frac{1}{r}\frac{\partial u'}{\partial \theta}\right) + \frac{1}{r}\frac{\partial(rf)}{\partial r}v' - w'\left(\frac{\partial u'}{\partial z} - \frac{\partial w'}{\partial r}\right) - \frac{\partial p'}{\partial r} + \frac{d}{R_o}\frac{1}{Re}\left(\nabla^2 u' - \frac{u'}{r^2} - \frac{2}{r^2}\frac{\partial v'}{\partial \theta}\right) \tag{12}$$

$$\frac{\partial v'}{\partial t} = w'\left(\frac{1}{r}\frac{\partial w'}{\partial \theta} - \frac{\partial v'}{\partial z}\right) - u'\left(\frac{1}{r}\frac{\partial r(f+v')}{\partial r} - \frac{1}{r}\frac{\partial u'}{\partial \theta}\right) - \frac{1}{r}\frac{\partial p'}{\partial \theta} + \frac{d}{R_o}\frac{1}{Re}\left(\nabla^2 v' + \frac{2}{r^2}\frac{\partial u'}{\partial \theta} - \frac{v'}{r^2}\right) \tag{13}$$

$$\frac{\partial w'}{\partial t} = u'\left(\frac{\partial u'}{\partial z} - \frac{\partial w'}{\partial r}\right) - (f+v')\left(\frac{1}{r}\frac{\partial w'}{\partial \theta} - \frac{\partial v'}{\partial z}\right) - \frac{\partial p'}{\partial z} + \frac{d}{R_o}\frac{1}{Re}\nabla^2 w' \tag{14}$$

where

$$\nabla^2 = \frac{1}{r}\frac{\partial}{\partial r}\left(r\frac{\partial}{\partial r}\right) + \frac{1}{r^2}\frac{\partial^2}{\partial \theta^2} + \frac{\partial^2}{\partial z^2} \tag{15}$$

The quantity f is the same as that defined in equation (3) and represents the nondimensional mean flow. It is computed using double precision to ensure sufficient accuracy. The Reynolds number used here is the same as that defined by equation (4). The relationship between (u',v',w',p') and (u,v,w,p) of section 2 is

$$\begin{aligned} u' &= u/Re \\ v' &= v \\ w' &= w/Re \\ p' &= p \end{aligned} \tag{16}$$

The boundary conditions are periodic in the azimuthal and axial directions. All velocity components are required to be zero at the inner and outer channel walls.

To solve these equations, we used a curved channel variant of the program described by Zang and Hussaini (refs. 7 and 8). It employs Fourier expansions in the θ and z directions and Chebyshev expansions in r. The independent variables are advanced in time by using Crank-Nicholson for the diffusion, pressure gradient, and incompressibility constraint terms, and third-order Runge-Kutta for the remaining terms. The CFL number limitation due to the stability of the Runge-Kutta method is $\sqrt{3}/\pi$. The pressure is computed on a staggered grid, and an advanced splitting method described by Zang and Hussaini (ref. 8) is used to reduce the errors at the walls. The methods require the solution of a Poisson equation for the pressure, and Helmholtz equations for the velocity components. Typically, at the end of a full time step, either the incompressibility constraint or the no-slip boundary condition is satisfied, but not both. However, our code enforces boundary conditions on the intermediate steps such that the error due to splitting the equations is reduced to

$O\left(\Delta t^2\right)$. (See Zang and Hussaini (ref. 8) for details.) The Helmholtz equations are solved with a Chebyshev tau method and the pressure equation by an iterative approach.

The spatial derivatives are approximated with analytic derivatives of the series representations. The nonlinear terms are evaluated most efficiently in physical space. Fast Fourier and Chebyshev transforms permit the data to be rapidly converted to and from its physical and spectral space representations. In this approach, as with other collocation methods, both truncation and aliasing errors are present. Canuto, Hussaini, Quarteroni, and Zang (ref. 9) discuss both types of errors in detail and provide a thorough discussion of available spectral algorithms for channel flow simulations. Recently, Zang (ref. 10) demonstrated that numerical simulations using collocation schemes experience smaller aliasing errors when the nonlinear convective terms are written in the skew-symmetric form rather than the rotation form. In the simulations discussed here, the skew-symmetric form has been used. On a 64^3 grid, the code uses approximately 90 μsec per grid point per step on a single Cray-2 processor.

The DNS code was extensively tested before being used for this project. Linear eigenmodes for both Dean and TS disturbances were obtained from a linear stability code used by DHZ. This code employs 501 grid points in a finite-difference method developed by Malik, Chuang, and Hussaini (ref. 11). At the critical curvature parameter $\lambda_c = 2.179 \times 10^{-5}$, 2D TS complex growth rates from the curved channel linear stability code differ from the corresponding quantities obtained from a straight channel spectral Orr-Sommerfeld solver by approximately 0.1%. A comparison of instantaneous complex growth rates from the DNS code with those obtained by the curved channel stability code is shown in table I. All cases were performed at the critical curvature ratio. The DNS data were obtained by using 48 Chebyshev modes in the radial direction. Initial amplitudes were 1.0×10^{-8} of the mean flow centerline velocity. The growth rates and frequencies were obtained after 100 time steps with $\Delta t = 10^{-5}$. Differences between the linear theory and the DNS are more pronounced for the TS waves ($m \neq 0$) than for the Dean disturbances ($m = 0$), but in all cases the differences are within the uncertainty range of the linear code.

Table I. Complex Growth Rates

Re	m	k	Linear stability code	Direct numerical simulation
75 500	0	9.02	0.4170	0.4166
75 500	74 600	0	(1.88, −4048.2)	(1.96, −4048.2)
80 700	0	1.50	1.5918	1.5916
80 700	73 160	0	(2.12, −3885.2)	(2.19, −3885.2)
80 698	73 160	1.59	(−26.49, −4844.9)	(−26.37, −4845.0)

Additional tests also indicate that the program provides accurate results in the nonlinear regime. Another curved channel simulation code written by Zang uses an unsplit procedure (ref. 7) for solving the Navier-Stokes equations. When started with identical initial conditions, using a time step of $\Delta t = 10^{-6}$, both the split and the unsplit codes indicated that instantaneous complex growth rates agreed to about 0.1% at four check points during 400 step simulations. These cases were in the nonlinear regime (the maximum streamwise perturbation was 7.2% of the mean centerline velocity), hence the instantaneous growth rates were not constant. One further check on the accuracy of the split code was obtained for $\eta = 0.975$, $Re = 2466$, $m = 15$, and $k = 5$. Here a nonlinear, nonaxisymmetric wave became periodic with a frequency of 3.095. Using a completely independent simulation code, Finlay et al. (ref. 12) obtained a frequency of 3.094. These tests give us confidence that our program accurately simulates curved channel flow.

4. Comparison of Results

Here we compare the predictions of the weakly nonlinear theory of DHZ with the results of DNS. The number of modes used to resolve the velocity in each direction was chosen to ensure well-resolved results.

In all the simulations the time step (for a full Runge-Kutta step) was $\Delta t = 10^{-5}$. The resultant CFL numbers in the simulations were all well below the Runge-Kutta stability limit; most were less than half the limit. For cases in which a TS wave was included, approximately 155 full Runge-Kutta steps were taken for each TS wave period.

Sufficient spatial resolution in the simulation can be ensured by using the guideline suggested by Krist and Zang (ref. 13). They suggest that "grid refinement is needed in any direction when the tail of the energy spectrum reaches 10^{-8} of the low-frequency value." This guarantees that truncation errors in the velocity will be less than 0.01%. Such detailed resolution is not necessary for the purposes of these simulations, though unless otherwise specified, the Krist and Zang guideline was followed. In what follows, M Chebyshev modes imply that there are $M+1$ Chebyshev collocation points across the channel; N Fourier modes imply that there are N collocation points in the given direction so that the Fourier wave numbers n have a range of $-N/2+1 \leq nL/(2\pi) \leq N/2-1$, where L is the length of the domain. Typically, 48 Chebyshev modes are used to resolve the flow in the wall-normal (radial) direction. In the streamwise (azimuthal) and spanwise (axial) directions, either 2, 6, or 12 Fourier modes were used, depending on the purpose of the given simulation. The code is structured such that at least two modes must be used in each direction. In cases where no TS mode is included, two modes are used in the streamwise direction. Similarly, where no Dean mode is included, two modes are used in the spanwise direction.

All cases considered perturbations from the neutrally stable point: $R_0 = 75\,000$, $\lambda = \lambda_c = 2.179 \times 10^{-5}$, $m = 74\,600$, and $k = 9.02$. The corresponding dimensional streamwise wave number was $d \cdot \alpha_{TS} = 1.62$. When the curvature ratio was perturbed, the simulations were performed keeping the value of $d \cdot \alpha_{TS}$ constant. Qualitatively similar results were obtained at other base Reynolds numbers. The cases presented here are considered representative of other parameter sets. For the work reported here, the values of the Landau coefficients corresponding to equations (9) and (10) are

$$\beta_1 = 0.908 \times 10^{-3} \qquad \beta_2 = 0.355 \times 10^{-2}$$

$$\delta_1 = -0.623 \times 10^{6} \qquad \delta_2 = -0.744 \times 10^{7}$$

$$\eta_1 = 0.118 \times 10^{2} \qquad \eta_2 = -0.851 \times 10^{-3}$$

$$\gamma_1 = 0.155 \times 10^{7} \qquad \gamma_2 = 0$$

Both positive and negative perturbations to the critical curvature ratio were studied. Each is presented separately.

4.1. Positive Curvature Perturbation

Here the weakly nonlinear theory predicts that TS and Dean modes can attain individual equilibrium states, but should they both be present initially, the TS mode will decay and the Dean mode will reach its steady state. Unless otherwise specified, the simulations here had $\epsilon^2\Lambda = 10^{-7}$ and $Re = R_0 + \epsilon^2 R_1 = 75\,500$. In order to keep the streamwise wave number $d \cdot \alpha_{TS}$ the same as that at the critical curvature ratio, equation (8) was used to obtain $m = 74\,257$. This value of m was used for all simulations at this curvature ratio. Three separate situations were considered: (1) only a Dean disturbance, (2) only a TS wave, and (3) both Dean and TS modes. Note that both TS and Dean modes are linearly unstable in this range.

When only a Dean disturbance is included as part of the initial conditions, the weakly nonlinear theory suggests that an equilibrium state ought to be obtained. From equation (9) with the

left-hand side equal to zero and $|Y|^2 = 0$, we can easily derive the equilibrium state, $\epsilon^2|X|^2 = -(\epsilon^2 R_1\beta_1 + \epsilon^2\Lambda\gamma_1)/\delta_1$. The corresponding rms value of the streamwise velocity component on the centerline is $v'_{\rm rms} = \epsilon|X|\sqrt{2} = 1.41 \times 10^{-3}$. We initiated the simulation with the Dean eigenfunction obtained from the linear stability code with an initial strength equal to that predicted by the weakly nonlinear theory. Its rms velocity components are given in figure 3. Twelve Fourier modes were used in the spanwise direction, though half the modes had energies which were more than 8 orders of magnitude less than the primary mode. These higher order modes had a negligible effect on the simulation. At the start of the simulation, the instantaneous growth rate of the Dean disturbance was approximately equal to its linear value, 0.57. As the simulation progressed, the growth rate continually decreased. At time $t = 0.13825$, the instantaneous growth rate was 0.07 and the simulation was stopped with the centerline streamwise rms velocity $v'_{rms} = 1.36 \times 10^{-3}$. In this case, the difference between the equilibrium state predicted by the weakly nonlinear theory and that obtained from the DNS is less than 5% and is considered quite good.

Initializing this flow with only a TS wave leads to the TS equilibrium state. From equation (10) with $|X| = 0$ and $\epsilon^2|Y|^2 = -(\epsilon^2 R_1\beta_2 + \epsilon^2\Lambda\gamma_2)/\eta_2$, one finds the rms value of the radial velocity component on the centerline is $u'_{\rm rms} = \epsilon|Y|\sqrt{2} = 8.56 \times 10^{-4}$. The simulation was initiated with $u'_{\rm rms} = 8.27 \times 10^{-4}$ and was stopped at time $t = 0.7465$ when the growth rate had slowed to 0.0018. At this time, the centerline vertical rms velocity is $u'_{\rm rms} = 9.52 \times 10^{-4}$. Figure 4 illustrates the time evolution of the amplitude of the wave. Note that as the amplitude approaches its equilibrium value, the growth rate decreases. Over 480 periods of the TS wave were simulated for the data presented in figure 4. The equilibrium amplitude predicted by the weakly nonlinear theory is shown by the dashed line. The difference between the equilibrium amplitude predicted by the weakly nonlinear theory and that obtained by the DNS is about 15%, which is considered acceptable agreement by Philip Hall. The 12 Fourier modes used in the streamwise direction were sufficient for an 8-order-of-magnitude drop in the energy.

We performed several simulations with both Dean and TS perturbations included in the initial conditions. In these, we typically used 6 modes in both the streamwise and the spanwise directions. As usual, 48 Chebyshev modes were used in the wall-normal direction. In these simulations, the spanwise resolution was only sufficient to allow an energy drop of 10^5, while the streamwise resolution allowed as little as a 10^4 drop in the energy. This would lead us to suspect errors in the velocity on the order of 1%. To determine whether this could lead to erroneous physical results, we resimulated our case which had the largest velocity perturbations, using 12 modes in the streamwise and spanwise directions and 64 modes in the wall-normal direction. The energy spectrum in the highly resolved case exhibited an energy drop of 10^9 in the streamwise direction and 10^{14} in the spanwise direction. The evolution of the disturbance amplitudes was the same as that observed in the less resolved case.

In the remaining parts of this subsection, unless otherwise specified, we initiated the Dean disturbances with $v'_{\rm rms} = 1.41 \times 10^{-3}$ on the centerline. This value is slightly more than its equilibrium amplitude which we obtained above. The weakly nonlinear theory predicts that for the given conditions, the Dean disturbance will evolve towards this equilibrium state.

In the first case, the initial strength of the TS disturbance was $u'_{\rm rms} = 6.93 \times 10^{-5}$, approximately 1/12 its predicted equilibrium value. The long time behavior of this case required 12 Fourier modes in the spanwise direction. The amplitude evolution of the disturbances is illustrated in figure 5(a). Here we plot the amplitude of both the Dean and TS disturbances, normalized by their respective amplitudes at time $t = 0$. The Dean disturbance develops towards its equilibrium state while the TS disturbance decays. This behavior is exactly what one would expect from the weakly nonlinear theory.

In the second case, the initial strength of the TS disturbance was $u'_{\rm rms} = 6.93 \times 10^{-4}$, approximately 5/6 its predicted equilibrium value. Figure 5(b) shows the amplitude histories for this case. Unlike the previous situation, here the TS wave grows slightly and the Dean disturbance experiences rapid decay. The decay of the Dean disturbance is not predicted by the weakly nonlinear theory. In an attempt to understand this discrepancy we look at the rms distribution of velocities

in the Fourier mode which characterizes the Dean disturbance in figure 6. Note that the vertical component of velocity has two local maxima in its distribution, and the spanwise component has three local maxima. Figure 3 illustrates the velocity components at time $t = 0$. Here the vertical and spanwise velocities have one and two local maxima, respectively. At the end of the simulation, the TS rms velocity distributions were the same as they were initially. In the previous case with the weaker TS wave, the Dean disturbance maintained its original structure throughout the simulation. The stronger TS disturbance in the present simulation distorts the cross-stream velocities in the Dean mode. Without the appropriate cross-stream velocity distribution, the streamwise velocity component of the Dean mode decays. Note that this happens quickly; the data in figure 5(b) represent approximately 15 TS wave periods. We continued this simulation with 12 modes in the streamwise direction. As seen in figure 7, the flow develops into a state with the TS wave at its equilibrium amplitude. Another case including both TS and Dean modes of comparable amplitude, but with $\epsilon^2 R_1 = 100$ and $\epsilon^2 \Lambda = 10^{-8}$, evolved similarly.

Another simulation was performed with precisely the same initial conditions as were used in the above paragraph. Instead of allowing the Dean disturbance to evolve naturally in time, we artificially forced its original amplitude and velocity distribution to be constant. Figure 8 shows the development of both the Dean and the TS disturbances. Unlike the previous case, here the TS disturbance decays in time, as one would expect from the weakly nonlinear theory. This indicates that the decay of the TS mode is directly linked to the presence of a strong, self-sustaining Dean vortex.

One more case of interest is when the Reynolds number perturbation is 2000, i.e., $Re = R_0 + \epsilon^2 R_1 = 77\,000$. The perturbation from the critical curvature ratio remained $\epsilon^2 \Lambda = 10^{-7}$. Initially the amplitudes of the Dean and TS disturbances are such that for their respective disturbances, $v'_{\text{rms}} = 1.38 \times 10^{-3}$ and $u'_{\text{rms}} = 9.70 \times 10^{-4}$ on the centerline. Figure 9 illustrates the energy in the Dean mode, the TS mode, and the oblique mode with wave vector ($m = 74\,257$, $k = 9.02$). Here energy is plotted instead of the magnitude of velocity at a single point in the channel. Since this case initially evolves quite similarly to the case above in which strong Dean and TS disturbances were allowed to develop, the velocity distribution in the Dean mode changes its structure in time, so the integrated energy in each mode is a much better measure of its size. Before $t \approx 0.08$, the drastic changes in the slope of the energy-versus-time plot for both the Dean and the oblique modes are correlated with large changes in the relative magnitudes of the streamwise and wall-normal components of the velocity in the Dean mode. The reason(s) for these changes is (are) not understood. For $t > 0.08$, both the oblique and the Dean modes become more energetic at approximately the same rate. This is due to a secondary instability similar to that described by Herbert (refs. 14 and 15) for the plane channel. According to the secondary instability theory, the oblique mode and the mode corresponding to the Dean vortex become unstable when the amplitude of TS disturbance exceeds some critical value that depends on the Reynolds number, the spanwise wave number, and the geometry of the flow. As can be seen from our results, this secondary instability is quite strong and will likely lead to the development of turbulence in the flow. Unlike the case above in which the TS mode achieved an equilibrium state before its amplitude was great enough to support a secondary instability for the spanwise wave numbers simulated, no simple equilibrium or periodic states are likely to develop in this flow.

An additional simulation was performed to investigate the possibility that higher order modes which are included in the simulation but not in the weakly nonlinear theory could be responsible for the discrepancy. The theory includes contributions from the Dean fundamental and first harmonic, the TS fundamental and first harmonic, the mean flow distortion, and the interaction between the Dean fundamental and the TS fundamental. These modes were allowed to evolve as usual. The modes corresponding to the interaction of either harmonic with either fundamental or each other were artificially set to zero at every time step. In this way, only the modes which the theory explicitly considers were permitted to evolve in the simulation. We initialized a simulation with the TS disturbance approximately equal to its equilibrium state and obtained results which were

qualitatively similar to what we had without suppressing any modes; the Dean mode decayed rapidly and the TS mode remained approximately constant.

4.2. Negative Curvature Perturbation

We explored one case in which the perturbation to the channel curvature was the opposite of that used above. With $\epsilon^2\Lambda = -1.0 \times 10^{-7}$ and $Re = 75\,100$, the weakly nonlinear theory predicts that the combined TS-Dean mode state dominates. As before, the value of m needed to be adjusted to keep $d \cdot \alpha_{\mathrm{TS}}$ constant. Using equation (8), we found $m = 74\,942$. Using these parameters, the linear growth rate of the TS wave is 0.33, while that of the Dean mode is -0.10. Weakly nonlinear theory predicts a combined equilibrium state with the Dean $v'_{\mathrm{rms}} = 3.08 \times 10^{-4}$ and the TS $u'_{\mathrm{rms}} = 1.68 \times 10^{-6}$.

The simulation was done using six modes in both the streamwise and the spanwise directions. The energy spectrum showed a drop of 10^{12} in the streamwise direction and 10^6 in the spanwise direction. In view of our experience with the positive curvature perturbation cases, this resolution was deemed sufficient for the purpose of determining the existence of a combined mode state. The amplitudes of the respective modes, divided by their initial amplitudes, are illustrated in figure 10. The Dean disturbance decays at the rate of -0.11, slightly faster than its linear rate obtained from the finite-difference code. The growth rate of the TS disturbance is 0.22, slightly less than its linear rate. The DNS does not indicate that a combined mode state exists with these parameters. It is possible that such a state exists with amplitudes of the respective disturbances somewhat different from those predicted by DHZ; however, the computational cost of finding such a state without additional information would be excessively high.

5. Discussion

Comparison of the results of the weakly nonlinear theory of DHZ with the results of DNS indicates that the theory and the simulation disagree with respect to some aspects of the flow.

When the curvature parameter perturbation of the channel is positive, any small, positive Reynolds number perturbation allows equilibrium states for isolated Dean and TS modes. The amplitudes of these states obtained with the weakly nonlinear theory and the DNS agree to acceptable accuracy. When both modes are included as part of the initial conditions, the weakly nonlinear theory predicts that the ultimate state will contain only a Dean mode in equilibrium; the TS mode is predicted to decay to zero. The DNS results indicate that this will occur if the initial Dean amplitude approximates its equilibrium amplitude and the TS amplitude is small. When the TS amplitude is close to its equilibrium state, the cross-stream velocity perturbations in the Dean mode lose their coherence and the Dean amplitude decays. If the structure and amplitude of the Dean mode are artificially maintained in their original condition, the TS mode will decay even though its initial amplitude is not small. We suggest two possible sources of this discrepancy: (1) the cases simulated were out of the range of validity of the theory, or (2) one of the Landau coefficients in equations (9) and (10) is incorrect. We discuss each of these possibilities below.

All weakly nonlinear theories suffer uncertainty as to their range of validity. There is no a priori way of knowing this range; it can only be checked a posteriori by comparison with some higher order theoretical predictions, physical experiments, or computations. The DHZ theory perturbs both the Reynolds number and the curvature ratio. In the cases presented above, the Reynolds number perturbation was 500 from a base Reynolds number of 75 000; the curvature parameter perturbation was 0.01×10^{-5} from a critical value of 2.179×10^{-5}. The Dean mode also decayed for a case with much smaller Reynolds number and curvature ratio perturbations. While it is possible for the perturbations used to be outside the valid range of the theory, such a limited range of validity would give the theory little predictive or explanatory value.

A numerical error in the calculation of one of the Landau coefficients in DHZ could explain the discrepancy between the theory and the DNS. Since equilibrium amplitudes of both Dean and TS

disturbances agree with the two approaches, it seems likely that the coefficients β_1, γ_1, δ_1, β_2, γ_2, and η_2 are approximately correct. When the Dean mode maintains itself (either artificially or because the TS mode is too weak to have a large impact on it), both the theory and the DNS agree that TS disturbances decay; hence, the coefficient responsible for the effect of the Dean mode on the TS mode, δ_2, seems to be correct. The DNS and the weakly nonlinear theory disagree on the effect of the TS mode on the Dean mode. This is felt only through η_1, hence it is possible that η_1 was computed incorrectly.

A numerical error in the computation of η_1 would also help explain the discrepancy between the predictions of the weakly nonlinear theory and the DNS for the case of negative curvature ratio perturbations. In the parameter range simulated, the weakly nonlinear theory predicts that both TS and Dean modes should coexist. The Dean mode by itself decays; there is no Dean equilibrium state. Only the influence of a TS wave, felt through the coefficient η_1, could make the sustained existence of a Dean mode possible. The DNS results do not indicate that the two modes coexist in equilibrium for the set of parameters studied. As before, the value of η_1 seems to be behind the discrepancy.

6. Conclusions

We performed direct numerical simulations (DNS) of curved channel flow in order to validate the weakly nonlinear theory of Daudpota, Hall, and Zang (DHZ). The two approaches provide amplitudes of equilibrium states for individual Dean and Tollmien-Schlichting (TS) disturbances which agree to acceptable accuracy. Unfortunately, the theory and the DNS are in conflict as to the effects of interaction between the two modes. Two possible sources of the disagreement have been discussed. It is possible that the weakly nonlinear theory is valid only for a very narrow range of parameters and that its use here is out of that range. A more likely possibility is indicated by the character of the discrepancies, which suggests that the effect of the TS disturbance on the Dean mode is not being correctly predicted by the theory. The reverse interaction, that of the Dean on the TS, does seem to be correctly predicted; hence, we believe that while the bulk of the theory was done correctly, the Landau coefficient, which reflects the influence of the TS on the Dean, was incorrectly calculated by DHZ.

NASA Langley Research Center
Hampton, VA 23665-5225
June 27, 1989

References

1. Dean, W. R.: Fluid Motion in a Curved Channel. *Proc. Royal Soc. London,* vol. 121, no. A787, Nov. 1, 1928, pp. 402–420.
2. Gibson, R. D.; and Cook, A. E.: The Stability of Curved Channel Flow. *Q. J. Mech. & Appl. Math.,* vol. 27, pt. 2, May 1974, pp. 149–160.
3. Daudpota, Q. Isa; Hall, Philip; and Zang, Thomas A.: On the Nonlinear Interaction of Görtler Vortices and Tollmien-Schlichting Waves in Curved Channel Flows at Finite Reynolds Numbers. *J. Fluid Mech.,* vol. 193, Aug. 1988, pp. 569–595.
4. Stuart, J. T.: On the Non-Linear Mechanics of Wave Disturbances in Stable and Unstable Parallel Flows. Part 1. The Basic Behaviour in Plane Poiseuille Flow. *J. Fluid Mech.,* vol. 9, pt. 3, Nov. 1960, pp. 353–370.
5. Watson, J.: On the Non-Linear Mechanics of Wave Disturbances in Stable and Unstable Parallel Flows. Part 2. The Development of a Solution for Plane Poiseuille Flow and for Plane Couette Flow. *J. Fluid Mech.,* vol. 9, pt. 3, Nov. 1960, pp. 371–389.
6. Bender, Carl M.; and Orszag, Steven A.: *Advanced Mathematical Methods for Scientists and Engineers.* McGraw-Hill Book Co., c.1978.
7. Zang, Thomas A.; and Hussaini, M. Yousuff: Numerical Experiments on Subcritical Transition Mechanisms. AIAA-85-0296, Jan. 1985.
8. Zang, Thomas A.; and Hussaini, M. Yousuff: On Spectral Multigrid Methods for the Time-Dependent Navier-Stokes Equations. *Appl. Math. & Comput.,* vol. 19, 1986, pp. 359–372.
9. Canuto, Claudio; Hussaini, M. Yousuff; Quarteroni, Alfio; and Zang, Thomas A.: *Spectral Methods in Fluid Dynamics.* Springer-Verlag, c.1988.
10. Zang, Thomas A.: On the Rotation and Skew-Symmetric Forms for Incompressible Flow Simulations. *Appl. Numer. Math.,* vol. 6, 1990.
11. Malik, M. R.; Chuang, S.; and Hussaini, M. Y.: Accurate Numerical Solution of Compressible Linear Stability Equations. *Z. Angew. Math. & Phys.,* vol. 33, no. 2, Mar. 1982, pp. 189–201.
12. Finlay, W. H.; Keller, J. B.; and Ferziger, J. H.: Instability and Transition in Curved Channel Flow. *J. Fluid Mech.,* vol. 194, Sept. 1988, pp. 417–456.
13. Krist, Steven E.; and Zang, Thomas A.: *Numerical Simulation of Channel Flow Transition—Resolution Requirements and Structure of the Hairpin Vortex.* NASA TP-2667, 1987.
14. Herbert, Thorwald: Stability of Plane Poiseuille Flow—Theory and Experiment. *Fluid Dyn. Trans.,* vol. 11, 1983, pp. 77–126.
15. Herbert, Thorwald: Secondary Instability of Plane Channel Flow to Subharmonic Three-Dimensional Disturbances. *Phys. Fluids,* vol. 26, no. 4, Apr. 1983, pp. 871–874.

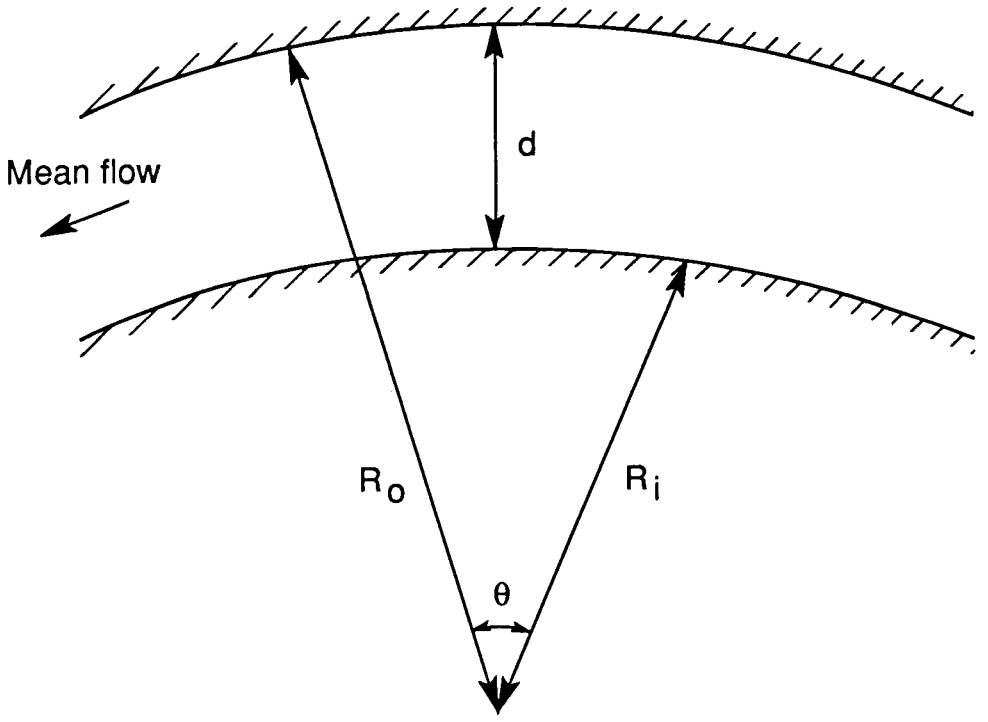

Figure 1. Curved channel flow geometry.

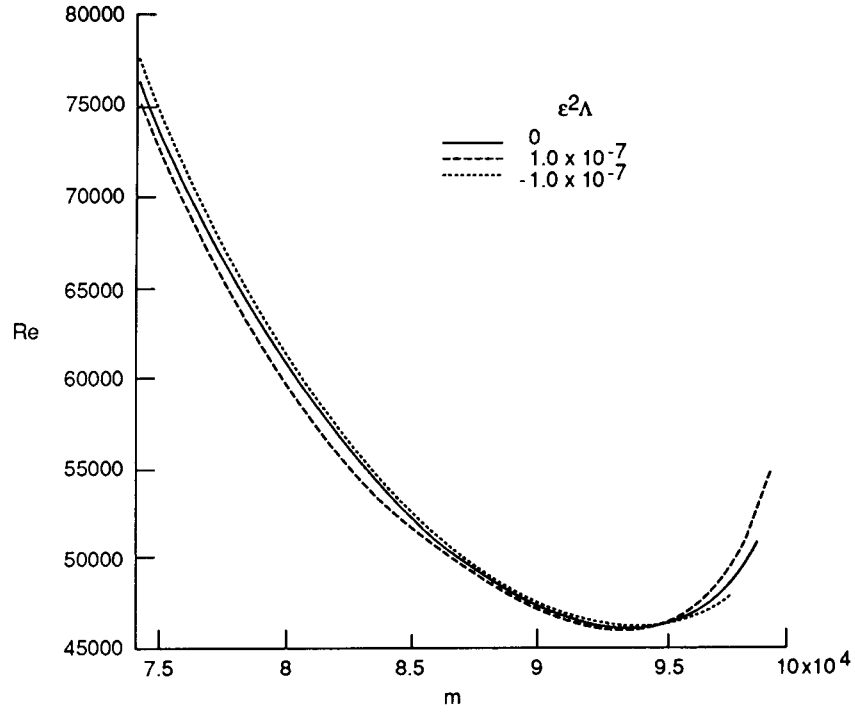

(a) TS disturbances.

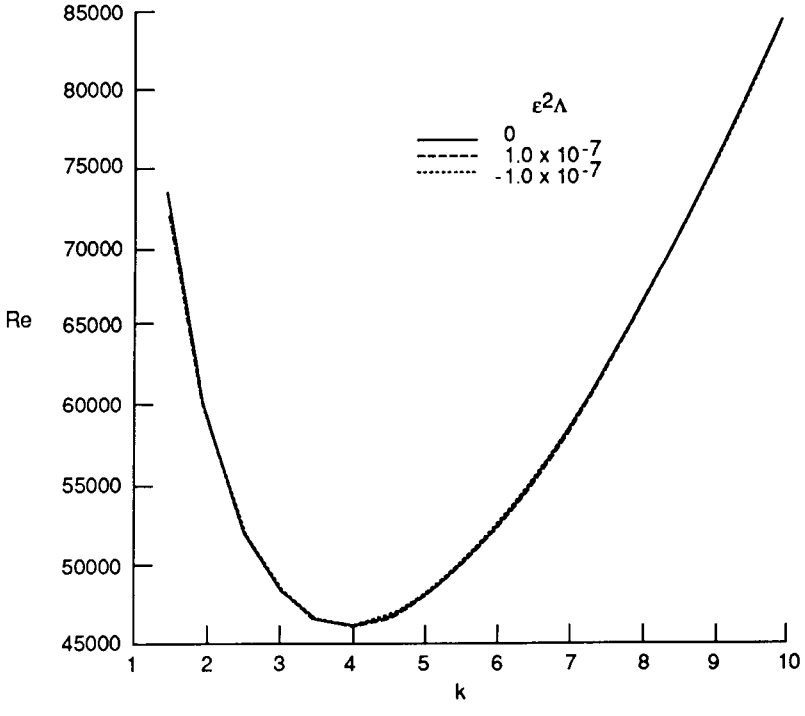

(b) Dean disturbances.

Figure 2. Neutral stability curves.

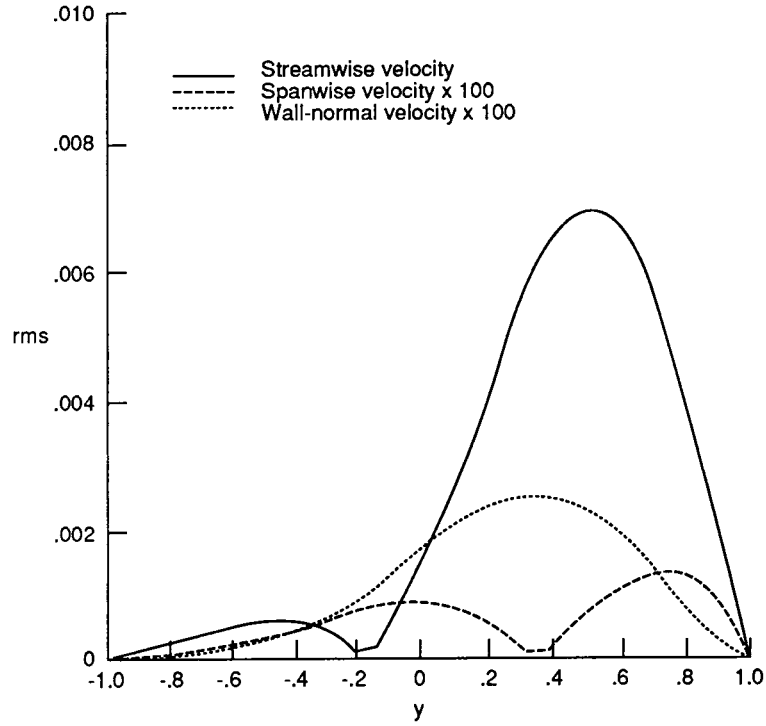

Figure 3. Initial distribution of rms velocity in the Dean mode. $Re = 75\,500; \epsilon^2\Lambda = 10^{-7}$.

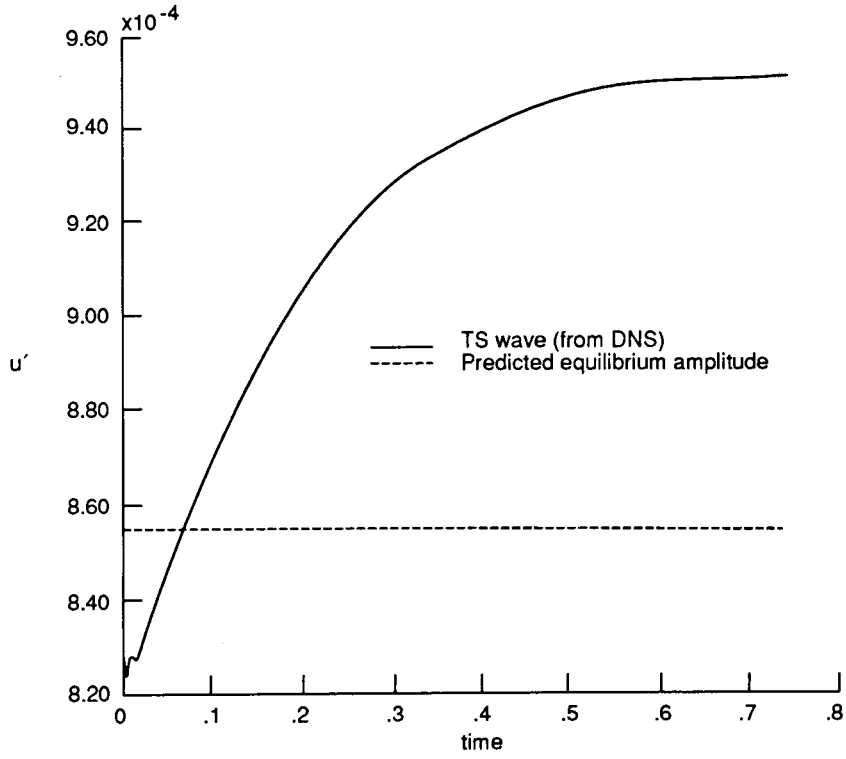

Figure 4. Amplitude evolution of TS wave.

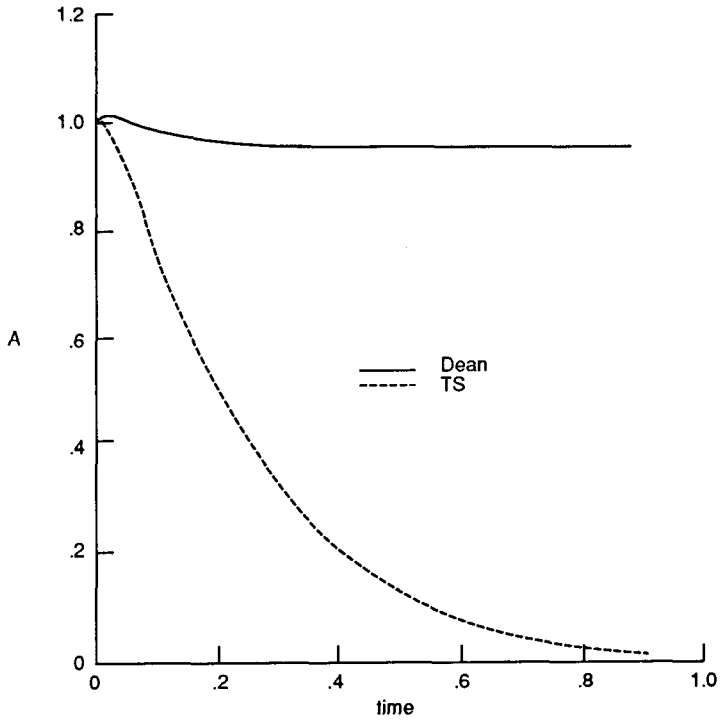

(a) Initial TS amplitude is approximately 1/12 its predicted equilibrium amplitude.

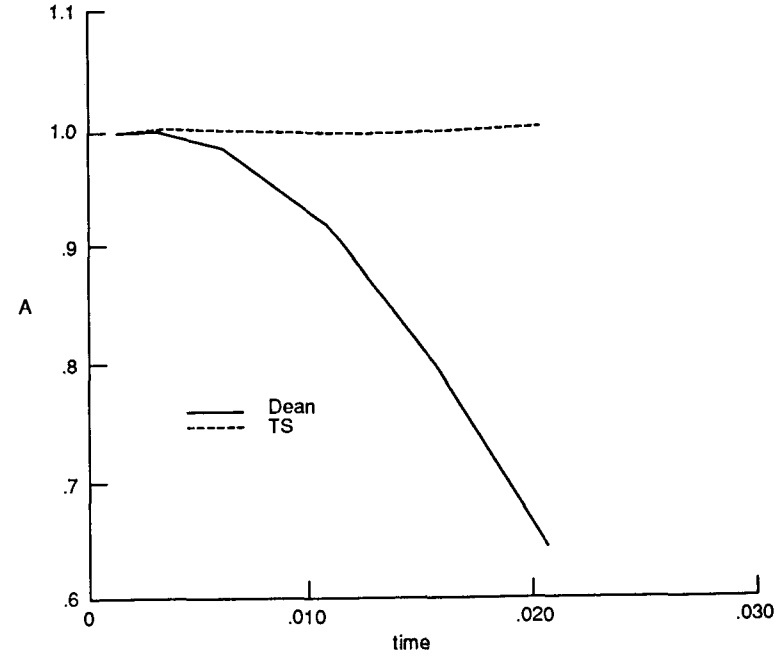

(b) Initial TS amplitude is approximately 5/6 its predicted equilibrium amplitude.

Figure 5. Time history of amplitude of Dean and TS modes, where A is the amplitude normalized by the respective initial amplitude.

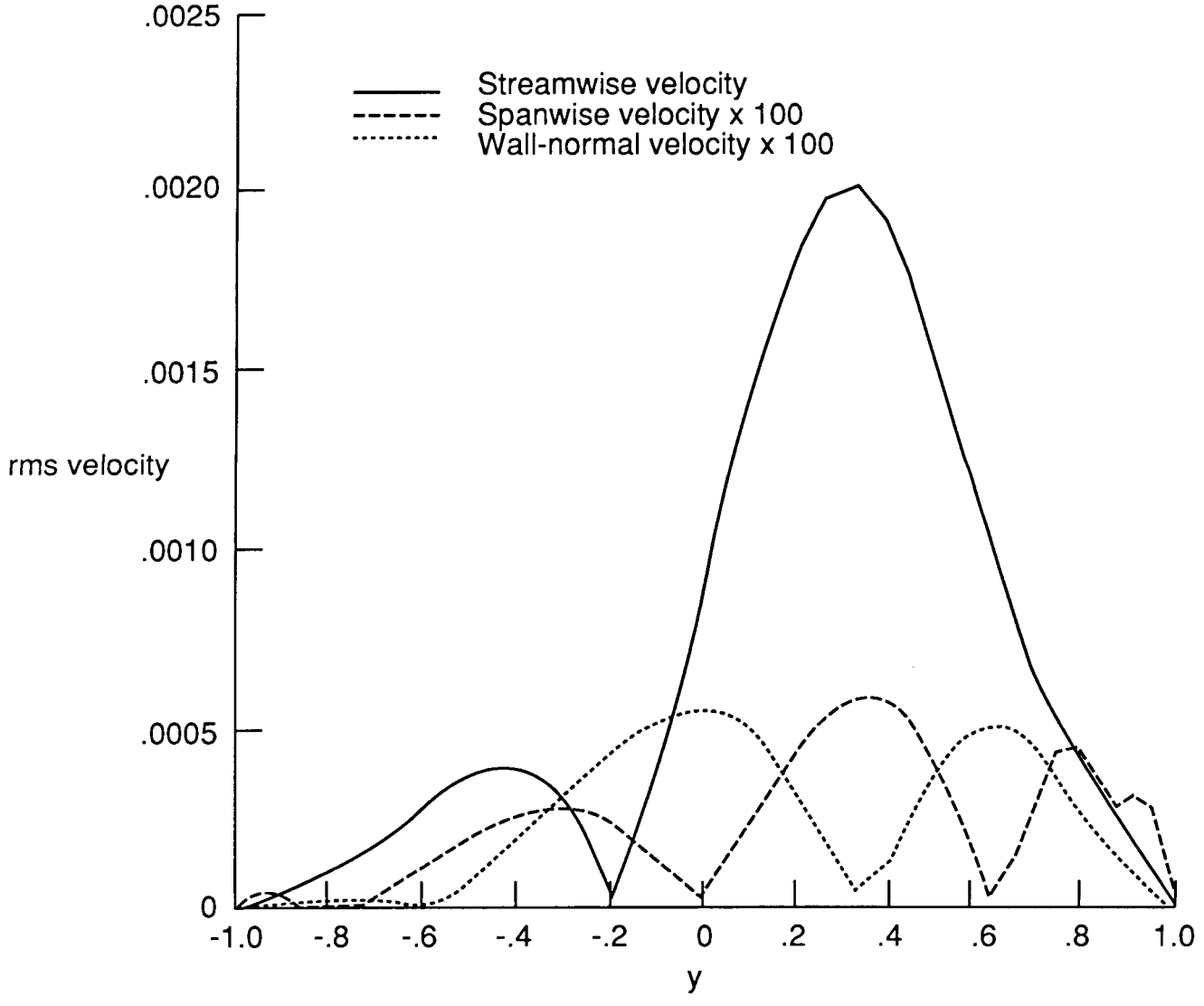

Figure 6. Rms velocity distribution in the Dean mode. $Re = 75\,500; \epsilon^2\Lambda = 10^{-7}; t = 0.021$; initial TS amplitude is approximately 5/6 its predicted equilibrium amplitude.

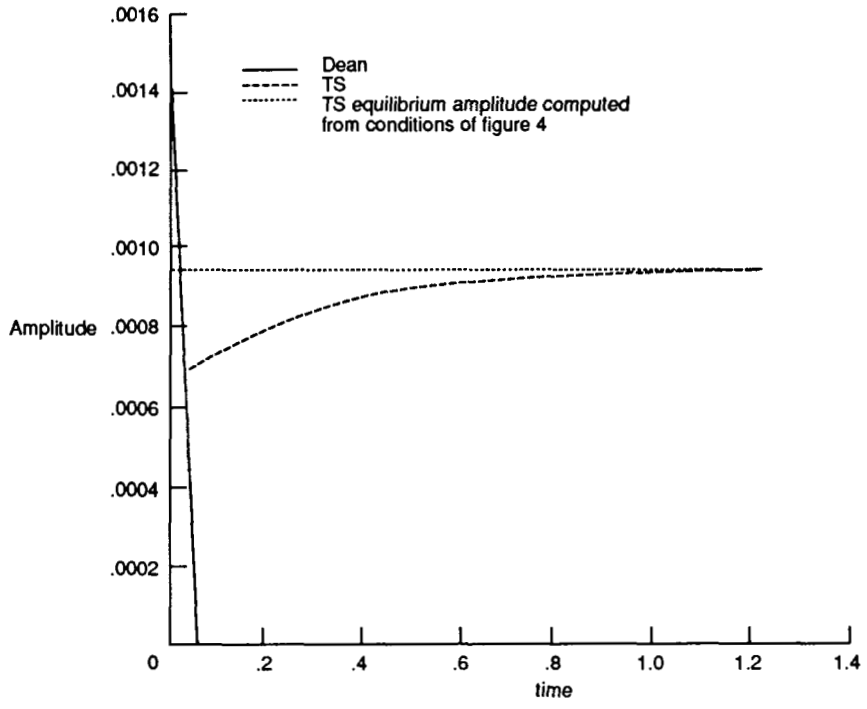

Figure 7. Long time amplitude evolution of Dean and TS modes for the conditions of figure 5(b).

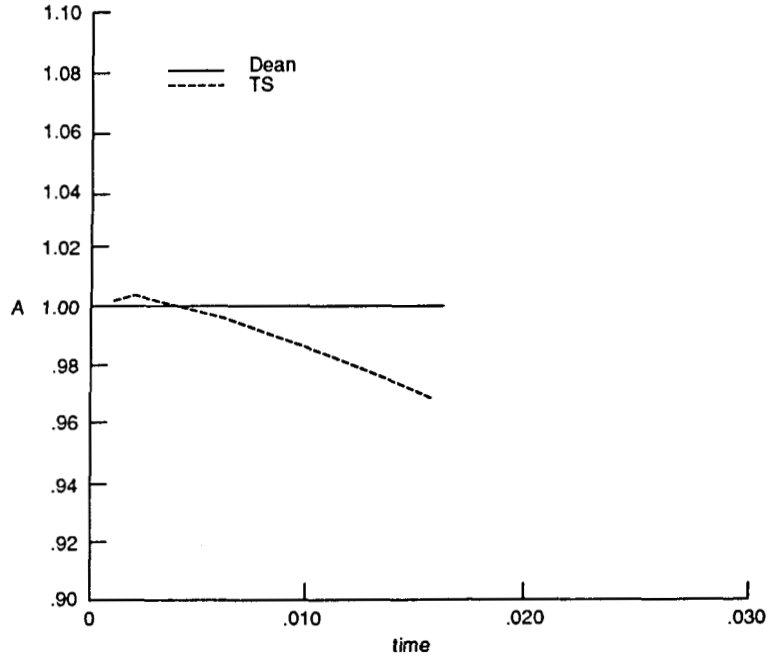

Figure 8. Time history of amplitude of Dean and TS modes, where A is the amplitude normalized by the respective initial amplitudes. Initial TS amplitude is approximately 5/6 its predicted equilibrium amplitude; the Dean disturbance is held constant in time.

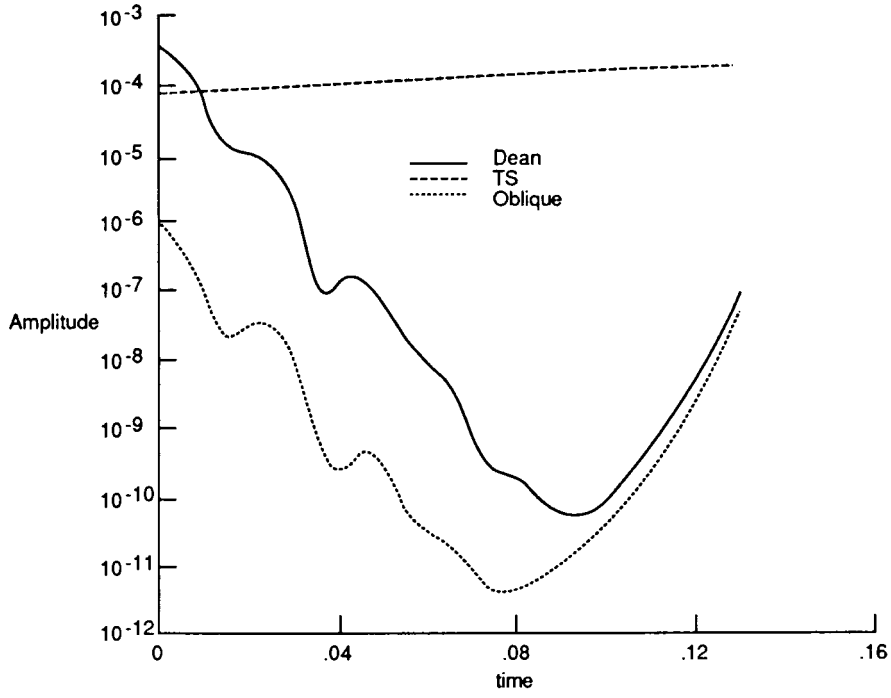

Figure 9. Time history of energy in Dean, TS, and oblique modes. $Re = 77\,000$.

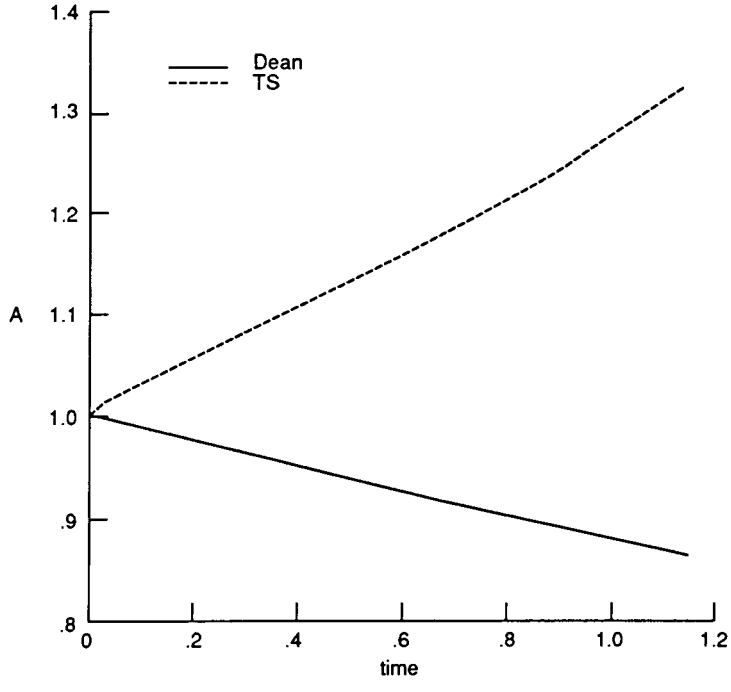

Figure 10. Time history of amplitude of Dean and TS modes, where A is the amplitude normalized by the respective initial amplitudes. $Re = 75\,100; \epsilon^2\Lambda = -1.0 \times 10^{-7}$; weakly nonlinear theory predicts a combined mode state.

NASA
National Aeronautics and Space Administration

Report Documentation Page

1. Report No.	2. Government Accession No.	3. Recipient's Catalog No.
NASA TP-2919		

4. Title and Subtitle
Interactions of Tollmien-Schlichting Waves and Dean Vortices
Comparison of Direct Numerical Simulations and a Weakly Nonlinear Theory

5. Report Date
August 1989

6. Performing Organization Code

7. Author(s)
Bart A. Singer and Thomas A. Zang

8. Performing Organization Report No.
L-16559

9. Performing Organization Name and Address
NASA Langley Research Center
Hampton, VA 23665-5225

10. Work Unit No.
505-60-01-02

11. Contract or Grant No.

12. Sponsoring Agency Name and Address
National Aeronautics and Space Administration
Washington, DC 20546-0001

13. Type of Report and Period Covered
Technical Paper

14. Sponsoring Agency Code

15. Supplementary Notes
Bart A. Singer: High Technology Corporation, Hampton, Virginia.
Thomas A. Zang: Langley Research Center, Hampton, Virginia.

16. Abstract

Direct numerical simulation is used to evaluate a weakly nonlinear theory describing the interaction of Tollmien-Schlichting waves with Dean vortices in curved channel flow. The theory and the simulation agree for certain combinations of parameters, but the two approaches give conflicting results for other combinations. Some possibilities for these discrepancies are discussed.

17. Key Words (Suggested by Authors(s))	18. Distribution Statement
Numerical simulation Transition Wave interactions	Unclassified—Unlimited Subject Category 02

19. Security Classif. (of this report)	20. Security Classif. (of this page)	21. No. of Pages	22. Price
Unclassified	Unclassified	19	A03

NASA FORM 1626 OCT 86
NASA-Langley, 1989
For sale by the National Technical Information Service, Springfield, Virginia 22161-2171